Published in final edited form as:
Cancer Res. 2013 August 15; 73(16): 5242–5252. doi:10.1158/0008-5472.CAN-13-0690.

Intratumoral Modeling of Gefitinib Pharmacokinetics and Pharmacodynamics in an Orthotopic Mouse Model of Glioblastoma

Jyoti Sharma[1,2], **Hua Lv**[2], and **James M. Gallo**[2]

[1]Department of Pharmaceutical Sciences, Temple University, 3307 N Broad Street, Philadelphia, PA, 19140, USA

[2]Department of Pharmacology and Systems Therapeutics, Mount Sinai School of Medicine, One Gustave L. Levy Place, New York, NY, 10029, USA

Abstract

Like many solid tumors, glioblastomas are characterized by intratumoral biological heterogeneity that may contribute to a variable distribution of drugs and their associated pharmacodynamics (PD) responses, such that that standard pharmacokinetic (PK) approaches based on analysis of whole tumor homogenates may be inaccurate. To address this aspect of tumor pharmacology, we analyzed intratumoral PK/PD characteristics of the EGFR inhibitor gefitinib in mice with intracerebral tumors and developed corresponding mathematical models. Following a single oral dose of gefitinib (50 or 150 mg/kg), tumors were processed at selected times according to a novel brain tumor sectioning protocol that generated serial samples to measure gefitinib concentrations, phosphorylated ERK and immunohistochemistry (IHC) in four different regions of tumors. Notably, we observed up to 3-fold variations in intratumoral concentrations of gefitinib, but only up to half this variability in pERK levels. Since we observed a similar degree of variation in the immunohistochemical index termed the microvessel pericyte index (MPI), a measure of permeability in the blood-brain barrier, we used MPI in a hybrid physiologically-based PK (PBPK) model to account for regional changes in drug distribution that were observed. Subsequently, the PBPK models were linked to a PD model that could account for the variability observed in pERK levels. Together, our tumor sectioning protocol enabled integration of the intratumoral PK/PD variability of gefitinib and IHC indices followed by the construction of a predictive PBPK/PD model. These types of models offer a mechanistic basis to understand tumor heterogeneity as it impacts the activity of anticancer drugs.

Keywords

Gefitinib; LC-MS/MS; MSD assay; mouse orthotopic glioblastoma model; intratumoral pharmacokinetics and pharmacodynamics; immunohistochemistry

Introduction

Glioblastoma multiforme (GBM), also called grade 4 astrocytoma, is the most aggressive and frequent of all primary brain tumors, accounting for about 54% of all gliomas (CBTRUS

Correspondence to: James M. Gallo, PhD., [2]Department of Pharmacology and Systems Therapeutics, Mount Sinai School of Medicine, One Gustave L. Levy Place, New York, NY, 10029, USA, Telephone: +212-241-7770; Fax: +212-996-7214; james.gallo@mssm.edu.

Conflict of interest: No potential conflict of interests were disclosed.

report 2011), with a median survival of less than 1 year from diagnosis (1, 2). Although new combination drug regimens have generated excitement and positive responses they ultimately fail as tumors enact numerous drug resistant mechanisms. These failures are often attributed to PD or cellular mechanisms that have their origins in either preexisting or adaptive genetic alterations that manifest as biochemical networks unresponsive to the selected drugs. Regional analysis from GBM samples has revealed extensive intratumoral heterogeneity in genetic composition and protein expression (3), including variable EGFRvIII expression (4), and EGFR and PDGFR gene amplification patterns across the same tumor sample (5). In such a scenario, reliance on singular bulk tumor samples to map individual genomic profiles and prioritize therapeutic strategies could be inaccurate as a means to advance personalized medicine.

In addition to PD-based treatment failures it is also reasonable to expect that PK-based failures also contribute to poor drug responses. In this case, tumor concentrations would be insufficient to inhibit intended targets that could be accentuated by intratumoral biological heterogeneity. Glioblastoma multiforme (GBM) is a heterogeneous highly invasive brain tumor characterized by a highly disorganized vasculature and a compromised blood-brain barrier (BBB) (6) Intratumoral variability within GBMs has been observed for morphology and functioning of the vasculature (7, 8), vessel permeability (9) interstitial fluid pressure (10), necrosis and cell proliferation and density (11, 12, 13, 14) that may contribute to heterogeneous drug distribution. Much of the limited data in this regard were based on the use of quantitative autoradiography, a sensitive technique that is limited by the resources need to synthesize radiolabeled drugs and their lack of specificity (10, 15, 16, 17, 18). Other attempts to examine regional PK variability have used unlabeled drugs and mass spectrometry for drug concentration measurements; however the measurements were sparse preventing a systematic analysis that would support the development of models (19). Of course it is to be expected that clinical investigations of brain tumor concentrations are limited by sample availability, yet there is an indication that intratumoral drug concentrations of various chemotherapeutic drugs (20, 21), and some targeted anticancer agents like imatinib (22) and gefitinib (23) were quite variable. All these studies lend support to the hypothesis that ineffective chemotherapy could be due to PK-based failures.

Given the rise in the importance of tumor heterogeneity and the lack of systematic investigations to detail such heterogeneity with respect to both PK and PD, we applied our recently developed tumor sampling protocol, which assigns adjacent tumor sections to either PK, PD or IHC analyzes, to characterize the intratumoral PK/PD variability of gefitinib.

Materials and Methods

Materials

U87/EGFRvIII and U87/PTEN cell lines were a generous gift from Dr. Webster Cavenee (University of California-San Diego) and Dr. Paul Mischel (UCLA), respectively. U87-MG cell line was purchased from the American Type Culture Collection. Authentication of cell lines, including the parental cell lines, was based on Western analyses of EGFR, EGFRvIII and PTEN. Gefitinib and the internal standard (IS) vandatinib were purchased from LC laboratories, Woburn, MA. All other chemicals and reagents were obtained from commercial suppliers as listed in the supplementary materials and methods.

Male NIH Swiss nude mice were supplied by Taconic Co. and maintained in the Center for Comparative Medicine and Surgery (CCMS) at Mount Sinai School of Medicine that is accredited by the Association for Assessment & Accreditation of Laboratory Animal Care, International (AAALAC). All animal studies were approved by the Institutional Animal

Care and Use Committee at Mount Sinai School of Medicine. Male nude mice at the age of 5–7 weeks and weighing 23 to 25 g were used for all studies.

Cell culture

U87, U87/PTEN and U87/EGFRvIII cells were cultured in DMEM with 10% fetal bovine serum and supplemented with 1x penicillin/streptomycin. The cells were maintained in a humidified incubator at 37°C with 5% CO2.

Orthotopic tumor implantation

The procedure for brain tumor implantation was similar to that reported previously (24). Briefly, nude mice (Male NIH Swiss nude mice, nu/nu, 5–7 weeks old) were anesthetized and secured in a stereotactic apparatus. A suspension of glioma cells (U87/EGFRvIII) was prepared fresh from culture (10^5 cells/μL in phosphate-buffered saline (PBS)) and injected (5 μL) into the caudate putamen. After 1 week, mice were monitored once a day for symptoms related to tumor growth that included an arched back, unsteady gait and loss of body weight. Mice were entered into the PK/PD studies when they showed a total body weight loss of 10% or more on two consecutive days.

In vivo gefitinib treatment and sampling

Gefitinib was administered at a dose of 50 or 150 mg/kg by oral gavage. A serial sacrifice design was used with blood and tumor samples collected from three mice at each scheduled time point [i.e. 0, 0.5, 1, 2, 4, 8, 18 and 24 hr] following drug administration. The brain tumors were serially sectioned using a cryostat to obtain samples for PK, PD and IHC analyses in four distinct regions separated by 1 mm intervals starting from the periphery (region R1) to the center (region R4) of each tumor as we recently reported (25).

Drug analysis (LC/MS/MS)

Previously validated LC/MS/MS methods were used to quantitate gefitinib in plasma (26) and brain tumor samples (25).

pERK analysis (MSD)

A highly sensitive electrochemiluminescence method was used to analyze pERK in brain tumor sections collected from various regions of brain tumor, as described previously (25). The assay was run according to the manufacturer's protocol with the phospho and total ERK ratios expressed as a fraction of baseline (untreated tumors) phospho/total ERK, which was set to 1.

Immunohistochemistry

Cryosections (12 μm) from frozen tumors were allowed to dry in air for 30 min followed by fixation in 4% methanol free paraformaldehyde (PFA) at room temperature. The sections were either triple stained with anti-CD31, anti-SMA and TUNEL (apoptosis) or double stained with anti-CD31 and anti-P-glycoprotein using diluted primary and secondary antibodies, followed by nuclear staining with DAPI. The detailed staining protocol can be found in the supplementary methods section.

The images of the cryosections were acquired (1.0 μm per pixel) as grayscale, using an automated fluorescent microscope (Zeiss Axioplan 2IE, Carl Zeiss Microscopy, Peabody, MA, USA) controlled by AxioVision software with subsequent image analyses processed by MetaMorph microscopy automation and image analysis software (Molecular Devices, Sunnyvale, CA, USA). The threshold values of each tumor section image were identified by positive staining and then semi-quantitated by measuring the number (for TUNEL/apoptosis

staining) or pixel area (for CD31 and SMA) of positive staining in the region of interest. The number of total TUNEL positive cells/total area of each selected region was presented as the number of apoptotic cells/mm2 of tissue area. Microvessel density (MVD) was calculated as the total CD31 positive pixel area × 100/total pixel area of the selected region. The microvessel pericyte index (MPI) required dual positive staining analysis of CD31 in combination with SMA as follows,

$$\text{MPI}=\frac{\text{Overlapping area of CD31 and SMA positive staining}}{\text{Total area of CD31 positive stain}}\times 100$$

The microvessel transporter index (MTI) that provided a measure of the efflux transporter Pgp expression on microvessels was similarly calculated as;

$$\text{MTI}=\frac{\text{Overlapping area of CD31 and Pgp positive staining}}{\text{Total are of CD31 positive stain}}\times 100$$

The images were pseudo-colored for presentation using Metamorph software.

PK and PD modeling

PK and PD data analyses were conducted with the SAAMII simulation and modeling program (version 2, University of Washington, WA). The analyses were based on a sequential modeling approach of first defining the PK models and then the PD models. A sequential modeling approach was also applied to obtain the PK models; specifically, hybrid physiologically-based PK (PBPK) models were derived by first fitting the model to the combined gefitinib plasma concentrations from both dose levels to obtain fixed forcing functions (see Table 1A) that were then used to fit the tumor models to the observed gefitinib tumor concentration data.

Based on the significant inverse correlation between gefitinib intratumoral concentrations and the MPI, three unique hybrid PBPK models of gefitinib were developed corresponding to three MPI groups, indicative of variable BBB permeability. In order to achieve this goal, the regional PK/PD data at each dose level was segregated into three groups according to their corresponding MPI values as shown in Fig. 1A. The MPI values in each tumor were ranked from 1 to 4. The tumor PK/PD measurements corresponding to regions with a MPI rank = 1 from both dose levels were grouped as the low MPI group, while those corresponding to regions with a MPI rank = 4 formed the high MPI data group. The data from the intermediate MPI ranks (2 and 3) were combined to obtain a medium MPI group. The PBPK models, consisting of a two compartment systemic disposition model and a two compartment permeability-limited brain tumor model, were individually fit for each MPI group to gefitinib intratumoral concentration data that produced three different sets of tumor PK parameters. The rate equations for the plasma forcing function and the tumor compartments are provided in the supplementary methods.

The following PK parameters were fixed based on previously reported values; oral absorption rate constant (K_a), oral bioavailability (26), and for the tumor PK models, tumor blood flow rate (Qt = 3ml/hr) (27)). The mean volume of tumor (V_t) was fixed as 0.001 ml based on its measured value and then assigned as the volume of tumor vascular compartment (V_v) and extravascular compartment (V_{ev}) based on a reported volume fraction (28, 29). The gefitinib tumor to plasma partition coefficient was determined as the average

of the ratio of observed tumor/plasma AUC (R) obtained from each dose level. The Michaelis-Menten constant (Km) for active efflux of gefitinib by P-glycoprotein (Pgp) at the BBB was estimated by using Bayesian constraints based on reported values (30). All other parameters were estimated by fitting the model to the observed gefitinib concentrations using maximum likelihood estimation. These parameters were; central compartment elimination rate constant (k_{10}), volume of distribution for the central compartment (V_c), intercompartment transfer rate constants (k_{12} and k_{21}), maximum rate of active efflux from tumor extravascular to vascular compartment (Vmax), tumor vascular to extravascular transcellular mass transfer co-efficient (h) and paracellular transport rate constant (K_p). Once the hybrid PBPK model was finalized, the associated PK variables were set as constant and linked to the PD model.

The fractional inhibition of pERK in tumors -using untreated tumors to obtain baseline pERK values- after gefitinib administrations was used as the PD response and represented as a three compartment sequence of a link compartment connected to a target (i.e. phosphorylated EGFR (pEGFR) – response (i.e. pERK) model. The link compartment consisted of an inhibitory Imax model to link gefitinib concentrations in tumor (C_t) to the PD model. The rate equations are provided in the supplementary methods.

It was assumed that the variability in the pERK response was solely driven by gefitinib tumor concentrations based on their slightly higher degree of variability that was attributed to changes in BBB permeability. It was necessary to segregate the PD models into low and high dose groups to obtain the best-fit models.

The PD model parameters estimated were the IC50 (gefitinib concentrations for 50% inhibition of pEGFR), K_{in} (the zero order formation rate for pEGFR), k_{tr} (the first order rate constant for signal propagation from the drug target pEGFR compartment to the response pERK compartment) and k_{out} (first order rate constant for degradation and dephosphorylation of pERK). The $pEGFR^0$ (the baseline level of tumor pEGFR) and Imax (the maximum inhibitory response of pEGFR) were fixed at 1. The best fit hybrid PBPK/PD models were evaluated according to the statistical criteria generated from SAAMII program that included the maximum likelihood objective function, the Akaike information criteria (AIC), and the precision of variables as measured by the coefficient of variation (CV%). In addition, diagnostic plots of model performance (observed data and residuals vs. model-predicted) are provided (Supplemental Fig. S6 and S7). The residual plots do not show systematic trends and ruled out model misspecification, yet even though differences in observed and predicted pERK values were at times large, the differences were random.

Results

Intratumoral PK/PD variability in gefitinib

A novel tumor sampling protocol was used to integrate PK, PD and IHC measurements from each tumor following administration of single doses of 50 mg/kg and 150 mg/kg of gefitinib to mice bearing intracerebral tumors. Tumor samples collected at the dose of 150 mg/kg gefitinib showed an intratumoral variability of gefitinib concentrations in the range of 1.2 to 2.4 fold over the entire 24 hr time course and about a 1.5 fold difference in the $AUC_{(0–24\ hr)}$ between the regions with highest and lowest gefitinib concentrations (Fig. 2A). In parallel to the regional tumor PK, corresponding PD (pERK) measurements varied 1.2–1.4 fold over 24 hours, with a similar area between the effect curves (ABEC), a measure of the cumulative degree of inhibition, between the regions with highest and lowest gefitinib concentrations (Fig. 2C). Although intratumoral variability at 150 mg/kg of gefitinib was low, gefitinib concentrations tended to increase moving from the tumor peripheral toward the central

regions, which produced an expected opposite trend in pERK values (Supplementary Fig. S1A, B).

Regional variability in intratumoral PK/PD in mice administered 50 mg/kg of gefitinib was slightly greater than at the higher dose level, and over 24 hours, gefitinib intratumoral concentrations ranged from 1.6-to 3-fold with a 2-fold difference in the $AUC_{(0–24\ hr)}$ in the regions with highest and lowest gefitinib concentrations (Fig 2B). The corresponding intratumoral PD variability was in the range of 1.2–1.9 fold, with a 1.4 fold difference in ABEC in the regions with highest and lowest gefitinib concentrations (Fig. 2D). Of some interest and opposite to the high dose trend, the gefitinib concentration gradient decreased in moving from the tumor peripheral towards the central regions (Supplementary Fig. S2A, B).

The viability of the tumor sampling protocol was demonstrated by use of another EGFRvIII brain tumor model, specifically the LN229/EGFRvIII-PTEN. Mice bearing these tumors were administered 150 mg/kg gefitinib orally and processed similar to the U87/EGFRvIII study. This preliminary study focused on the assessment of intratumoral variability in gefitinib concentrations that showed a similar degree of variability as in the U87EGFRvIII model; ranging from 1.6- to 3.2-fold intratumoral differences over the 24 hour sampling period (Supplementary methods, Supplementary Table S2).

Intratumoral variability in biological characteristics

In order to identify biological characteristics of the tumor that could explain the variability in gefitinib intratumoral concentrations, microvessel density, microvessel pericyte index and apoptotic cells (MVD, MPI and apoptotic cells/mm^2) in the tumor regions adjacent to the PK and PD measurements were analyzed; first in the high-dose 150 mg/kg group. There was a small but significant difference ($p < 0.05$) in the microvessel density (MVD) between the tumor peripheral and central regions, being lower at the tumor center (Fig. 3A–C), consistent with a previous report (31). It seemed counterintuitive that the regions with high MVD values had lower gefitinib concentrations; however the MPI, an index of microvessel pericyte coverage and a more accurate indicator of BBB integrity, showed significantly ($p < 0.05$) higher values in the tumor peripheral regions compared to the central regions (Fig. 3D–F), and inversely correlated with the gefitinib concentration gradient. There was no significant difference in the intratumoral apoptotic cells measurements as a function of tumor region, and this was not further considered as a potential determinant of drug distribution at the lower 50 mg/kg dose. Therefore, the integrity of the BBB as measured by the MPI was found to be the most significant determinant of gefitinib brain tumor distribution in the high dose group.

The MPI values in the low dose gefitinib group also showed significant ($p < 0.05$) intratumoral variability. Although, unlike the high dose group, the high MPI values were located more centrally (Supplementary Fig. S3A), but still showed an inverse correlation to the intratumoral gefitinib concentration gradient. Given the concurrence between MPI and intratumoral gefitinib concentrations at both dose levels (Fig. 4) we concluded that BBB integrity was the primary determinant of regional gefitinib tumor concentrations.

Since gefitinib is reported to be a substrate for P-glycoprotein (Pgp) (32), a small subset of tumors (n=4) from the 50 mg/kg dose level were stained for Pgp and quantified as the MTI (Microvessel Trasporter Index). MTI values indicated a significantly greater Pgp expression on microvessels in the tumor center as compared to the peripheral region. Also the regional MTI measurement and the corresponding MPI in each of these tumor regions showed a significant positive correlation, reflecting that tumor microvessels with a more intact BBB are associated with a greater Pgp expression (Supplementary Fig. S3B–I) and could be an additional factor responsible for variability in gefitinib PK/PD.

Regional PK/PD models of gefitinib based on differential BBB permeability

The best-fit PBPK models consisted of a two compartment systemic disposition model and a two compartment permeability-limited model for the tumor (Fig. 1B). The latter 2-compartment vascular-extravascular model attested to the importance of BBB integrity as a key determinant in gefitinib brain tumor distribution. Specifically, the tumor model incorporated passive transcellular diffusion, active efflux and passive paracellular transport processes. The active efflux term represented Pgp-mediated BBB efflux and was based on the more than dose-proportional increase in gefitinib AUC in tumor (Supplementary Table S1). Transcellular diffusion is a bidirectional process driven by concentration gradients across the BBB. Paracellular transport of gefitinib is a unique mechanism that accounted for unidirectional entry of protein-bound gefitinib across the disrupted BBB. The best-fit model supported this was not a bidirectional process. The disrupted BBB caused by the growth of the tumor created large endothelial cell gaps that are highly permeable to water soluble compounds and large molecular weight proteins like albumin (7). The size of the endothelial gaps is much larger than the steric diameter of albumin, and hence, could be a significant source of drugs like gefitinib that are highly bound to plasma proteins. In this case, plasma protein-bound gefitinib passing into the tumor interstitium could dissociate and form a dynamic equilibrium with unbound drug, and contribute to the pool of free drug able to traverse intracellularly and interact with its receptor or diffuse back into blood. The predicted plasma and tumor concentration-time profiles agreed well with the observed values in all three MPI (low, medium and high) data groups (Fig 5).

Several interesting findings supported our hypothesis that variable intratumoral BBB integrity was the primary mechanism for variability in the tumor PK of gefitinib (Table 1B). First, the predicted area under the tumor concentration-time curve (AUC) for gefitinib adhered to the following order, low MPI AUC > medium MPI AUC > high MPI AUC, consistent with the relationship between MPI and BBB integrity, especially at the low dose. This trend was slightly offset at the high gefitinib dose with the medium MPI AUC being minimally less than the AUC for the high MPI group. Second, the difference between the low and high MPI tumor AUC in the low dose group was greater (2 fold higher AUC in low MPI group) than in the high dose group where the low and high MPI tumor AUCs were more similar. One likely reason for this observation is that at the high dose of gefitinib, Pgp-mediated efflux at the BBB is saturated preventing any further increase in efflux at high concentrations. This phenomenon by allowing more gefitinib to penetrate the BBB may also have contributed to the lower intratumoral variability observed at the 150 mg/kg dose level. Third, Vmax values, indicative of the maximum P-gp mediated transport rate, were in the rank order of high MPI Vmax > medium MPI Vmax > low MPI Vmax that directly corresponded to the observation of lower Pgp expression found in the regions with low MPI (Supplementary Fig. S3B–I), and consistent with a previous report that found Pgp expression negatively correlated with immature cerebral capillaries (33). Finally, the transcellular diffusion coefficient, h, which is a product of BBB permeability and its surface area, was found to be almost 5-fold greater in the low MPI group as compared to the medium MPI group and 8-fold greater as compared to the high MPI group (low MPI ‘h’ > medium MPI ‘h’ > high MPI ‘h’), consistent with the low MPI regions having a more permeable vasculature due to poor pericyte coverage. The paracellular transport rate term (K_p) was not significantly different between the three MPI groups, indicating that its contribution is relatively constant across all MPI groups, and that the transcellular transport is the major contributor to the intratumoral PK variability.

Once the hybrid PBPK model for each MPI group was established, the models were linked to PD models that characterized the pERK profiles as shown in Fig. 1B. A three-compartment sequence of a link compartment connected to a target-response model (26) provided the best-fit PD model. Given our assumption that MPI-mediated differences in the

PBPK models drove changes in the pERK response, a separate PD model for each MPI group was not required. Instead, a PD model was fitted to the combined pERK data from all the MPI groups, yet segregated by dose (Supplementary Fig. S4 for each MPI group) generating two sets of PD model parameters (Table 1C). This approach attests to the similar pERK profiles for each MPI group. Attempts to fit PD models for each MPI group or for the combined pERK data for both dose levels resulted in less accurate fits than those based on dose level. The baseline pEGFR0 and Imax values were set equal to 1 based on the assumption that the phosphorylation of EGFR was not inhibited in the absence of gefitinib and that it could be fully inhibited at high gefitinib tumor concentrations, respectively. To reduce parameter estimation difficulties, the value of K_{in}, a variable representing the formation of pEGFR, was fixed in the low dose group to a value equal to that obtained from the high-dose PD model and indicated that the synthesis rate of pEGFR was not influenced by dose. The IC50 values were found to be dose-dependent with a higher value (3-fold) obtained at the 150 mg/kg dose level. The transfer rate constant, k_{tr}, a variable that reflects signal transduction efficiency from pEGFR to pERK showed an inverse relationship with dose indicative of reduced signaling efficiency at higher gefitinib concentrations. The model predicted area between effect curves (ABEC), which provides a measure of cumulative degree of inhibition (34), indicated there was minimal difference in the ABEC values as a function of the MPI groups in both the high and low dose groups; yet dose-dependent increases in the model-predicted ABEC values were obtained; being 1.26-fold, 1.24-fold and 1.15-fold for the high, medium and low MPI groups, respectively (Table 1C).

Discussion

Most preclinical pharmacokinetic/pharmacodynamics (PK/PD) studies in brain tumor bearing mice are based on measurements from whole tumor homogenates that rely on the assumption of homogeneous drug distribution (i.e. single averaged drug concentration) for interpretation. However, it is well known that tumors are heterogeneous with regard to vascularity, blood flow and interstitial fluid pressure, and more recently genomic characteristics that could impact both PK and PD variability, and ultimately, personalized medicine (5). As individualized medicine moves forward an accounting of intratumoral PK/PD heterogeneity is necessary to not only understand why drugs may be inactive, but further to offer computational approaches to mitigate the effects of tumor heterogeneity. Models of regional PK/PD provide a tool to design improved dosing schedules to attain therapeutically relevant PK concentrations in the entire tumor that will produce optimal PD effects. It can be appreciated that such PK/PD models will become increasingly important as multidrug combinations are designed that may be subject to drug-drug interactions, both in the PK sphere as well as in the PD sphere where drugs act on the same and intersecting cell signaling pathways. The current study characterized the intratumoral PK and PD characteristics of gefitinib, a model EGFR inhibitor, and as a first investigation in this area, began to unravel how such data may be modeled to enhance our understanding of intratumoral PK/PD.

A pivotal advance in our approach was to develop a tumor sampling scheme that was readily accessible and provided regional PK and PD measurements that could be related to biological characteristics of the tumor measured by IHC. Adjacent serial sections were assigned to either PK, PD or IHC analyses, and in this particular investigation, four such regions were obtained at 1 mm intervals in the coronal direction. Both gefitinib concentration and pERK measurements required about five adjacent 12 um tissue sections or about 1 mg of brain tumor, whereas IHC analyses could be completed on each 12 um section that were interdigitated between the PK and PD sections that served as a means to bin the PK and PD data. This procedure, by combining adjacent tissue sections, does lump or average the measurements, yet much less so than whole tumor homogenates, and with

potential improvements in assay sensitivities improved resolution can be expected. Overall, the tumor sectioning protocol permitted each animal to contribute regional PK/PD/IHC measurements that facilitated our understanding of tumor heterogeneity.

Prior to the PK/PD investigations in brain tumor-bearing mice, in vitro PD biomarker studies were conducted in U87vIII cells to confirm that pERK could be used as a PD marker (supplementary Fig S5). The in vivo studies were then completed at two dose levels to assess dose-dependent changes in intratumoral PK/PD; the high gefitinib dose of 150 mg/kg was based on previous preclinical studies that showed this dose to be the highest nontoxic oral dose, and a dose of 50 mg/kg was chosen based on previous studies related to gefitinib's interactions with Pgp, at the BBB (32). Since the brain tumor vasculature has been reported to show regional variability in Pgp expression (higher at the tumor periphery) (35), it was important to include Pgp in our analysis.

The orthotopic brain tumor model possessed mutant EGFR (EGFRvIII) that is more sensitive to gefitinib than the widely used parental line, U87MG. The EGFRvIII variant has been reported to form a discreet well circumscribed intracerebral tumor mass, with a more aggressive phenotype than the U87MG tumors (36), and hence, more likely to recapitulate the phenotype of brain tumors in patients. The intratumoral variability of gefitinib PK ($AUC_{(0–24\ hr)}$) was about 2-fold, and comparable to a 3-fold intratumoral variability reported for gefitinib brain tumor concentrations in a single patient receiving a multiple-dose regimen of 500 mg/day (23). The slightly lower intratumoral variability in gefitinib brain tumor concentrations observed at the 150 mg/kg gefitinib dose could be attributed to saturation of efflux transporters at the BBB, and thus, limit Michaelis-Menten transport that is sensitive to concentration changes, and likely to exhibit greater variability. The variability in the intratumoral concentrations of gefitinib did not directly translate into the same degree of PD variability based on pERK measurements that were fairly uniform especially after high dose administration (Fig. 2C), and could indicate gefitinib brain tumor concentrations were sufficiently high to produce near maximal inhibition of pERK. Although pERK regional variability was modest it should be appreciated that drugs that exhibit steep concentration-response curves will be prone to greater variability; apparently the gefitinib concentration-pERK relationship in U87vIII tumors is not.

The tumor vasculature exhibited significant intratumoral variability and was depicted according to MPI values. Many studies have reported the role of pericytes in regulating vascular integrity and maturity via regulation of endothelial cell proliferation, formation of tight junctions, and the composition of the extracellular matrix (ECM) around vessels (37–39). The negative correlation obtained between MPI and gefitinib concentrations indicated that a more mature or functionally intact BBB (higher MPI) was a factor that impaired the delivery of gefitinib to brain tumors. Antiangiogenic treatment can influence tumor distribution of coadministered drugs; both increased and decreased drug delivery has been reported, which is related to a so-called vascular normalization process associated with increased pericyte coverage, decreased permeability and IFP (24, 40, 41, 42). Although our study design prevents drawing directly from these analyses we do show that a more functionally intact BBB limits gefitinib distribution into tumors, which is in agreement with previous reports on gefitinib brain distribution (43, 44).

The PK characteristics of gefitinib were most different in the low and high MPI groups that were explained by different BBB transport, and in terms of model parameters were attributed to transcellular diffusion (i.e. h) and active efflux by Pgp (Vmax). Both parameters, h and Vmax, were found to be MPI-dependent which is consistent with previous reports that pericytes regulate vascular integrity and maturity (37–39). One of these studies showed that the lack of pericyte coverage was associated with destabilized and permeable

tumor vessels, resulting in increased metastasis (37–39). Another study demonstrated greater biotin leakage into mouse brain that was attributed to lower pericyte coverage of brain microvessels. These reports support our contention that higher transcellular diffusion would be expected in vessels with less pericyte coverage or low MPI. The Vmax dependence on MPI was consistent with the observed lower Pgp expression in the regions with low MPI and a previous report that found Pgp expression negatively correlated with immature cerebral capillaries (33). Paracellular transport (K_p) of gefitinib was independent of MPI status, which seems reasonable because the basis for paracellular transport of gefitinib is large endothelial cell gaps that are characteristic of the physically disrupted BBB found in brain tumors (45).

Tumor pERK profiles predicted by the model agreed with the observed results in the low and high dose groups in all MPI groups. The PD model showed a dose-dependent increase in IC50, a similar phenomenon that has been observed previously (46, 26, 47), yet not always attached to a definitive mechanism. In one case, a dose-dependent change in EC50 was reported when a single drug acted simultaneously on two different receptors or targets (48). In a similar context, although gefitinib is known for its highly selective and potent EGFR inhibition, it targets at least 20 other kinases, *albeit* with higher IC50 values than for EGFR. One such target is an at higher concentrations it inhibits another intracellular kinase called cyclin G-associated kinase (GAK) (49), that negatively regulates EGFR signaling, (50). By removing this negative feedback mechanism more gefitinib is required to inhibit the intended target (pEGFR), and thus, the higher IC50 value at the high dose level. We do not have direct evidence to support this mechanism but the plausibility of this dose-dependency was supported by the model.

In summary, the study successfully illustrates how intratumoral heterogeneity in the biological characteristics of the tumor can result in variable drug exposure and PD response, albeit to a limited extent in this case. Nonetheless, the ability to characterize regional PK/PD information from tumors, made accessible through a tumor sectioning protocol, is advantageous to understand potential reasons for drug inactivity that traditional PK/PD studies based on tumor homogenates cannot offer. By combining PK/PD/IHC measurements regional PBPK/PD models, highlighted by variable BBB integrity, were developed that had the drug's efficacy been under evaluation could be used to examine alternate dosing strategies to attain therapeutically relevant concentration and PD effects throughout the tumor. Intratumoral PK/PD models provide an additional means to improve chemotherapy for GBMs.

Supplementary Material

Refer to Web version on PubMed Central for supplementary material.

Acknowledgments

Financial support: This work was supported by NIH grants CA072937 and CA127963.

References

1. Iacob G, Dinca EB. Current data and strategy in glioblastoma multiforme. J Med Life. 2009; 2(4): 386–93. [PubMed: 20108752]
2. Louis DN, Ohgaki H, Wiestler OD, Cavenee WK, Burger PC, Jouvet A, et al. The 2007 WHO classification of tumours of the central nervous system. Acta Neuropathol. 2007; 114(2):97–109. [PubMed: 17618441]

3. Jung V, Romeike BF, Henn W, Feiden W, Moringlane JR, Zang KD, et al. Evidence of focal genetic microheterogeneity in glioblastoma multiforme by area-specific CGH on microdissected tumor cells. J Neuropathol Exp Neurol. 1999 Sep; 58(9):993–9. [PubMed: 10499441]
4. Bonavia R, Inda MM, Cavenee WK, Furnari FB. Heterogeneity maintenance in glioblastoma: A social network. Cancer Res. 2011; 71(12):4055–60. [PubMed: 21628493]
5. Little SE, Popov S, Jury A, Bax DA, Doey L, Al-Sarraj S, et al. Receptor tyrosine kinase genes amplified in glioblastoma exhibit a mutual exclusivity in variable proportions reflective of individual tumor heterogeneity. Cancer Res. 2012; 72(7):1614–20. [PubMed: 22311673]
6. Jain RK, di Tomaso E, Duda DG, Loeffler JS, Sorensen AG, Batchelor TT. Angiogenesis in brain tumours. Nat Rev Neurosci. 2007; 8(8):610–22. [PubMed: 17643088]
7. Schlageter KE, Molnar P, Lapin GD, Groothuis DR. Microvessel organization and structure in experimental brain tumors: Microvessel populations with distinctive structural and functional properties. Microvasc Res. 1999; 58(3):312–28. [PubMed: 10527772]
8. Weissleder R, Cheng HC, Marecos E, Kwong K, Bogdanov A Jr. Non-invasive in vivo mapping of tumour vascular and interstitial volume fractions. Eur J Cancer. 1998; 34(9):1448–54. [PubMed: 9849430]
9. Jain R, Gutierrez J, Narang J, Scarpace L, Schultz LR, Lemke N, et al. In vivo correlation of tumor blood volume and permeability with histologic and molecular angiogenic markers in gliomas. AJNR Am J Neuroradiol. 2011; 32(2):388–94. [PubMed: 21071537]
10. Vavra M, Ali MJ, Kang EW, Navalitloha Y, Ebert A, Allen CV, et al. Comparative pharmacokinetics of 14C-sucrose in RG-2 rat gliomas after intravenous and convection-enhanced delivery. Neuro Oncol. 2004; 6(2):104–12. [PubMed: 15134624]
11. Paulus W, Peiffer J. Intratumoral histologic heterogeneity of gliomas. A quantitative study. Cancer. 1989; 64(2):442–7. [PubMed: 2736491]
12. Coons SW, Johnson PC. Regional heterogeneity in the proliferative activity of human gliomas as measured by the ki-67 labeling index. J Neuropathol Exp Neurol. 1993; 52(6):609–18. [PubMed: 8229080]
13. Cheng LL, Anthony DC, Comite AR, Black PM, Tzika AA, Gonzalez RG. Quantification of microheterogeneity in glioblastoma multiforme with ex vivo high-resolution magic-angle spinning (HRMAS) proton magnetic resonance spectroscopy. Neuro Oncol. 2000; 2(2):87–95. [PubMed: 11303625]
14. Wagner M, Nafe R, Jurcoane A, Pilatus U, Franz K, Rieger J, et al. Heterogeneity in malignant gliomas: A magnetic resonance analysis of spatial distribution of metabolite changes and regional blood volume. J Neurooncol. 2011; 103(3):663–72. [PubMed: 21061143]
15. Horowitz M, Blasberg R, Molnar P, Strong J, Kornblith P, Pleasants R, et al. Regional [14C]misonidazole distribution in experimental RT-9 brain tumors. Cancer Res. 1983; 43(8): 3800–7. [PubMed: 6861144]
16. Lockman PR, Mittapalli RK, Taskar KS, Rudraraju V, Gril B, Bohn KA, et al. Heterogeneous blood-tumor barrier permeability determines drug efficacy in experimental brain metastases of breast cancer. Clin Cancer Res. 2010; 16(23):5664–78. [PubMed: 20829328]
17. Reyzer ML, Hsieh Y, Ng K, Korfmacher WA, Caprioli RM. Direct analysis of drug candidates in tissue by matrix-assisted laser desorption/ionization mass spectrometry. J Mass Spectrom. 2003; 38(10):1081–92. [PubMed: 14595858]
18. Gelderblom H, Verweij J, van Zomeren DM, Buijs D, Ouwens L, Nooter K, et al. Influence of cremophor el on the bioavailability of intraperitoneal paclitaxel. Clin Cancer Res. 2002; 8(4): 1237–41. [PubMed: 11948138]
19. Agarwal S, Mittapalli RK, Zellmer DM, Gallardo JL, Donelson R, Seiler C, et al. Active efflux of dasatinib from the brain limits efficacy against murine glioblastoma: Broad implications for the clinical use of molecularly-targeted agents. Mol Cancer Ther. 2012; 11(10):2183–92. [PubMed: 22891038]
20. Donelli MG, Zucchetti M, D'Incalci M. Do anticancer agents reach the tumor target in the human brain? Cancer Chemother Pharmacol. 1992; 30(4):251–60. [PubMed: 1643692]

21. Pitz MW, Desai A, Grossman SA, Blakeley JO. Tissue concentration of systemically administered antineoplastic agents in human brain tumors. J Neurooncol. 2011; 104(3):629–38. [PubMed: 21400119]
22. Holdhoff M, Supko JG, Gallia GL, Hann CL, Bonekamp D, Ye X, et al. Intratumoral concentrations of imatinib after oral administration in patients with glioblastoma multiforme. J Neurooncol. 2010; 97(2):241–5. [PubMed: 19768386]
23. Hofer S, Frei K. Gefitinib concentrations in human glioblastoma tissue. J Neurooncol. 2007; 82(2): 175–6. [PubMed: 17008949]
24. Zhou Q, Gallo JM. Differential effect of sunitinib on the distribution of temozolomide in an orthotopic glioma model. Neuro Oncol. 2009; 11(3):301–10. [PubMed: 18971416]
25. Sharma J, Lv H, Gallo JM. Analytical approach to characterize the intratumoral pharmacokinetics and pharmacodynamics of gefitinib in a glioblastoma model. J Pharm Sci. 2012; 101(11):4100–6. [PubMed: 22865095]
26. Wang S, Guo P, Wang X, Zhou Q, Gallo JM. Preclinical pharmacokinetic/pharmacodynamic models of gefitinib and the design of equivalent dosing regimens in EGFR wild-type and mutant tumor models. Mol Cancer Ther. 2008; 7(2):407–17. [PubMed: 18281523]
27. Sun Y, Schmidt NO, Schmidt K, Doshi S, Rubin JB, Mulkern RV, et al. Perfusion MRI of U87 brain tumors in a mouse model. Magn Reson Med. 2004; 51(5):893–9. [PubMed: 15122670]
28. Pathak AP, Kim E, Zhang J, Jones MV. Three-dimensional imaging of the mouse neurovasculature with magnetic resonance microscopy. PLoS One. 2011; 6(7):e22643. [PubMed: 21818357]
29. Gambarota G, Leenders W, Maass C, Wesseling P, van der Kogel B, van Tellingen O, et al. Characterisation of tumour vasculature in mouse brain by USPIO contrast-enhanced MRI. Br J Cancer. 2008; 98(11):1784–9. [PubMed: 18506183]
30. Ozvegy-Laczka C, Hegedus T, Varady G, Ujhelly O, Schuetz JD, Varadi A, et al. High-affinity interaction of tyrosine kinase inhibitors with the ABCG2 multidrug transporter. Mol Pharmacol. 2004; 65(6):1485–95. [PubMed: 15155841]
31. Jain RK. Delivery of molecular and cellular medicine to solid tumors. Adv Drug Deliv Rev. 2001; 46(1–3):149–68. [PubMed: 11259838]
32. Agarwal S, Sane R, Gallardo JL, Ohlfest JR, Elmquist WF. Distribution of gefitinib to the brain is limited by P-glycoprotein (ABCB1) and breast cancer resistance protein (ABCG2)-mediated active efflux. J Pharmacol Exp Ther. 2010; 334(1):147–55. [PubMed: 20421331]
33. Sawada T, Kato Y, Sakayori N, Takekawa Y, Kobayashi M. Expression of the multidrug-resistance P-glycoprotein (pgp, MDR-1) by endothelial cells of the neovasculature in central nervous system tumors. Brain Tumor Pathol. 1999; 16(1):23–7. [PubMed: 10532420]
34. Sharma A, Jusko WJ. Characteristics of indirect pharmacodynamic models and applications to clinical drug responses. Br J Clin Pharmacol. 1998; 45(3):229–39. [PubMed: 9517366]
35. Fellner S, Bauer B, Miller DS, Schaffrik M, Fankhanel M, Spruss T, et al. Transport of paclitaxel (taxol) across the blood-brain barrier in vitro and in vivo. J Clin Invest. 2002; 110(9):1309–18. [PubMed: 12417570]
36. Nishikawa R, Ji XD, Harmon RC, Lazar CS, Gill GN, Cavenee WK, et al. A mutant epidermal growth factor receptor common in human glioma confers enhanced tumorigenicity. Proc Natl Acad Sci U S A. 1994; 91(16):7727–31. [PubMed: 8052651]
37. Morikawa S, Baluk P, Kaidoh T, Haskell A, Jain RK, McDonald DM. Abnormalities in pericytes on blood vessels and endothelial sprouts in tumors. Am J Pathol. 2002; 160(3):985–1000. [PubMed: 11891196]
38. Daneman R, Zhou L, Kebede AA, Barres BA. Pericytes are required for blood-brain barrier integrity during embryogenesis. Nature. 2010; 468(7323):562–6. [PubMed: 20944625]
39. Raza A, Franklin MJ, Dudek AZ. Pericytes and vessel maturation during tumor angiogenesis and metastasis. Am J Hematol. 2010; 85(8):593–8. [PubMed: 20540157]
40. Goel S, Duda DG, Xu L, Munn LL, Boucher Y, Fukumura D, et al. Normalization of the vasculature for treatment of cancer and other diseases. Physiol Rev. 2011; 91(3):1071–121. [PubMed: 21742796]
41. Rustum YM, Toth K, Seshadri M, Sen A, Durrani FA, Stott E, et al. Architectural heterogeneity in tumors caused by differentiation alters intratumoral drug distribution and affects therapeutic

synergy of antiangiogenic organoselenium compound. J Oncol. 2010; 2010:396286. [PubMed: 20445750]

42. Tailor TD, Hanna G, Yarmolenko PS, Dreher MR, Betof AS, Nixon AB, et al. Effect of pazopanib on tumor microenvironment and liposome delivery. Mol Cancer Ther. 2010; 9(6):1798–808. [PubMed: 20515941]
43. McKillop D, Hutchison M, Partridge EA, Bushby N, Cooper CM, Clarkson-Jones JA, et al. Metabolic disposition of gefitinib, an epidermal growth factor receptor tyrosine kinase inhibitor, in rat, dog and man. Xenobiotica. 2004; 34(10):917–34. [PubMed: 15764411]
44. Fukuhara T, Saijo Y, Sakakibara T, Inoue A, Morikawa N, Kanamori M, et al. Successful treatment of carcinomatous meningitis with gefitinib in a patient with lung adenocarcinoma harboring a mutated EGF receptor gene. Tohoku J Exp Med. 2008; 214(4):359–63. [PubMed: 18441512]
45. Hashizume H, Baluk P, Morikawa S, McLean JW, Thurston G, Roberge S, et al. Openings between defective endothelial cells explain tumor vessel leakiness. Am J Pathol. 2000; 156(4): 1363–80. [PubMed: 10751361]
46. Bergeron L, Bevan DR, Berrill A, Kahwaji R, Varin F. Concentration-effect relationship of cisatracurium at three different dose levels in the anesthetized patient. Anesthesiology. 2001; 95(2):314–23. [PubMed: 11506100]
47. Derendorf H, Meibohm B. Modeling of pharmacokinetic/pharmacodynamic (PK/PD) relationships: Concepts and perspectives. Pharm Res. 1999; 16(2):176–85. [PubMed: 10100300]
48. Lundstrom J, Lindgren JE, Ahlenius S, Hillegaart V. Relationship between brain levels of 3-(3-hydroxyphenyl)-N-n-propylpiperidine HCl enantiomers and effects on locomotor activity in rats. J Pharmacol Exp Ther. 1992; 262(1):41–7. [PubMed: 1352554]
49. Brehmer D, Greff Z, Godl K, Blencke S, Kurtenbach A, Weber M, et al. Cellular targets of gefitinib. Cancer Res. 2005; 65(2):379–82. [PubMed: 15695376]
50. Zhang L, Gjoerup O, Roberts TM. The serine/threonine kinase cyclin G-associated kinase regulates epidermal growth factor receptor signaling. Proc Natl Acad Sci U S A. 2004; 101(28): 10296–301. [PubMed: 15240878]

A.

Tumor #	1	2	3	and so on..
	MPI Rank			
Tumor Region #				
R1	**1**	3	**4**	
R2	2	**4**	3	
R3	**4**	2	**1**	
R4	3	**1**	2	

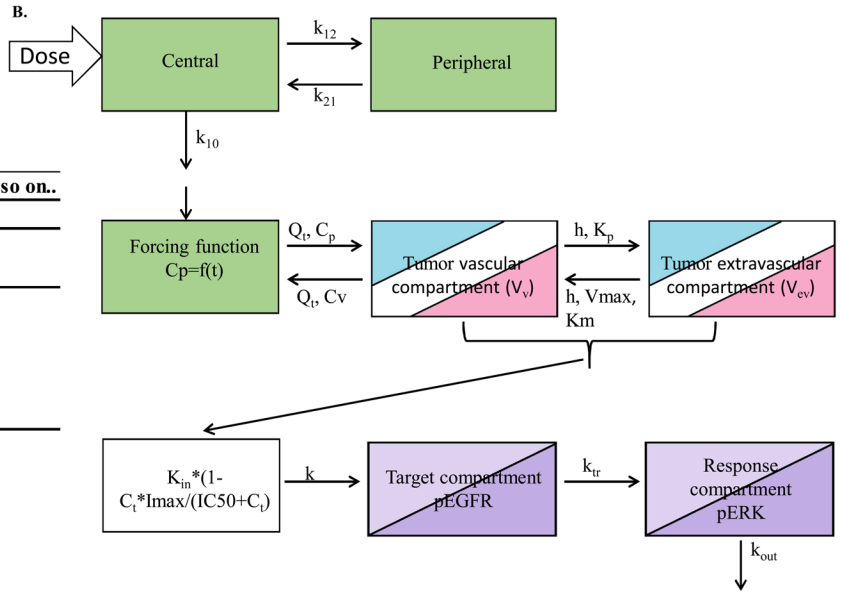

Figure 1.

Gefitinib intratumoral PK/PD modeling scheme. **A.** Schematic representation of intratumoral data segregation strategy based on regional MPI rank. Each of the four brain tumor regions in each mouse were assigned an MPI rank based on their measured values. The rank of 1 [highlighted in pink] formed the low MPI group, ranks of 2 and 3 formed the medium MPI group and the rank of 4 [highlighted in blue] formed the high MPI group. The gefitinib brain tumor-tumor concentrations and corresponding pERK values were binned according to the MPI rank. **B.** Schematic representation of a physiologically-based hybrid PK/PD model consisting of a two compartment systemic disposition model [green], a two compartment tumor model [3 colors for each MPI group], and a three compartment sequence of a link compartment connected to a target-response model [2 colors for low and high dose groups]. Parameters shown in systemic disposition model are; the elimination rate constant (k_{10}), intercompartment transfer rate constants (k_{12} and k_{21}), for the tumor model; blood flow rate to tumor (Q_t), maximum rate of active efflux from tumor extravascular to vascular compartment (Vmax), tumor transcellular transport rate constant (h), Michaelis-Menten constant (Km), and tumor vascular to extravascular paracellular transport rate constant (K_p), total gefitinib tumor concentration (Ct), and for the PD model; gefitinib tumor concentrations for 50% inhibition of pEGFR (IC50), the zero-order rate constant for formation of pEGFR (K_{in}), the first order rate constant for signal propagation from the drug target pEGFR compartment to the response pERK compartment (k_{tr}), and a first-order rate constant for degradation and dephosphorylation of pERK (k_{out}). The parameter “k” was used to link gefitinib tumor concentrations to the pEGFR target compartment and fixed at a value of 1. Refer to text for other model parameters and fitting procedure.

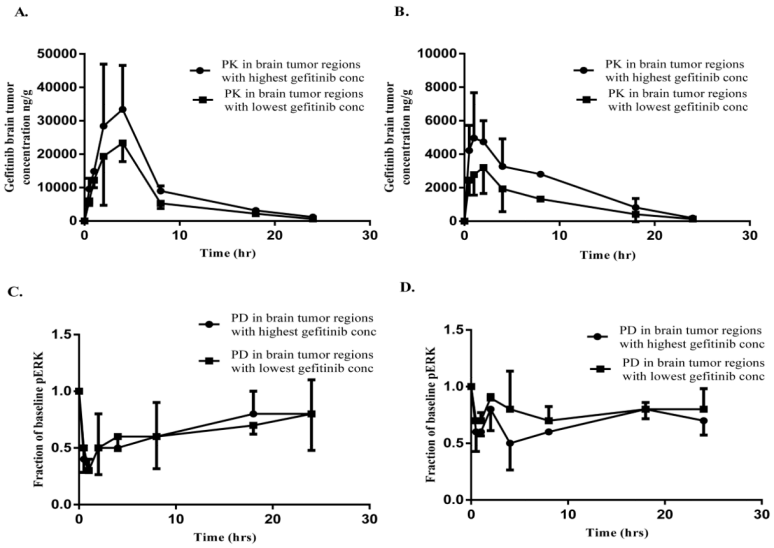

Figure 2.

Intratumoral variability in gefitinib PK/PD following single oral doses of 150 mg/kg and 50 mg/kg gefitinib to mice bearing intracerebral U87/vIII tumors. **A.** Gefitinib brain tumor concentrations at 150 mg/kg and **B.** 50 mg/kg and **C.** PD responses based on pERK (fraction of baseline pERK) at 150 mg/kg and **D.** 50 mg/kg, in the regions with the lowest and highest variability. All observed points represent the mean + or − SD.

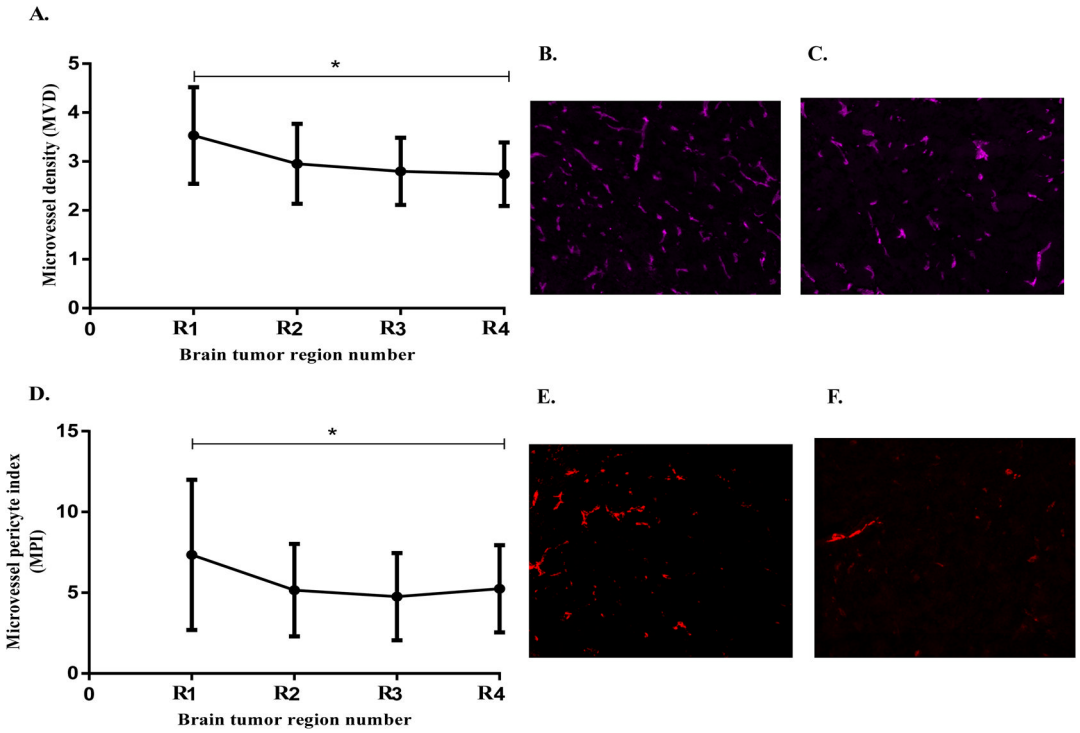

Figure 3.

Intratumoral immunohistochemical analysis of MVD and MPI in U87vIII brain tumors following single oral doses of 150mg/kg gefitinib; data points = mean ± SD values from each tumor region from all the animals in the study (n=21). **A**. Regional variability in MVD showing decreasing MVD values from tumor periphery to center ($p < 0.05$), **B and C**. Representative images of MVD (CD31 staining) at tumor periphery and center, respectively. **D.** Regional variability in MPI showing decreasing MPI values from tumor periphery to center (significant difference, $p < 0.05$), and **E and F**. Representative images of microvessel pericyte coverage (α-SMA staining) at tumor periphery and center, respectively. Each image was acquired as a grayscale image at a resolution of 1.0 μm per pixel and then pseudo-colored for presentation.

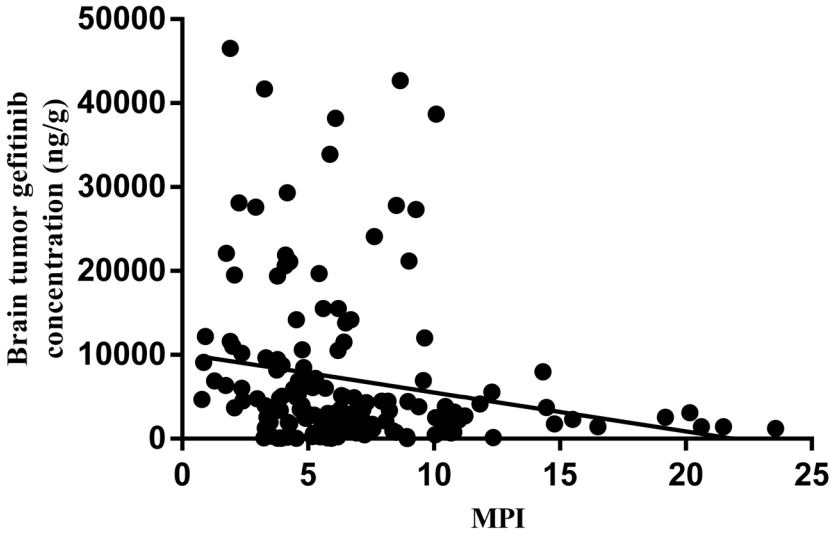

Figure 4.

Regional gefitinib brain tumor concentrations as a function of the corresponding regional MPI (as determined by immunohistochemical analysis) values following single doses of 50 mg/kg and 150 mg/kg gefitinib orally (all mice and regions included). A significant negative correlation was found, Pearson correlation coefficient = −0.19, P= 0.014.

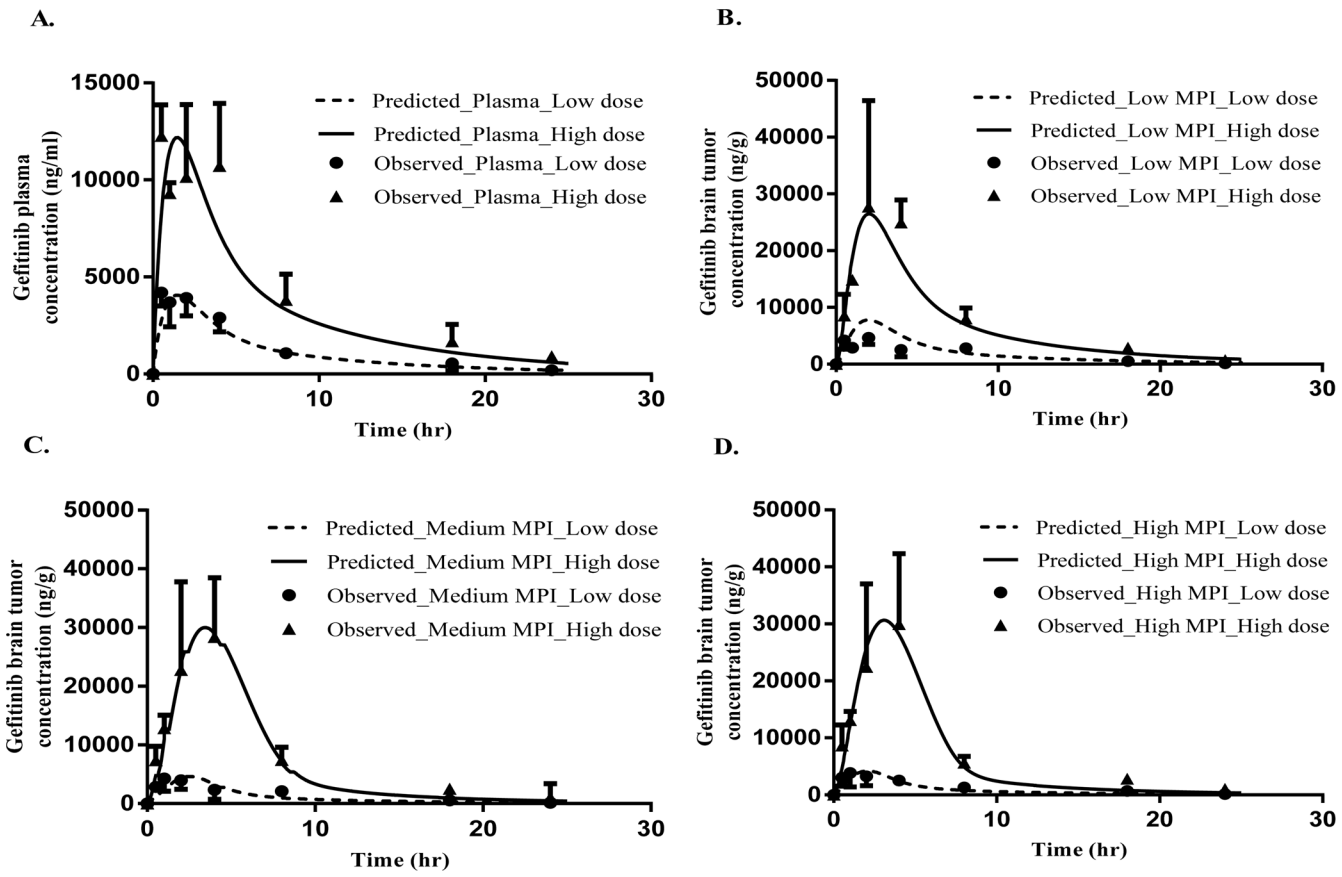

Figure 5.

Intratumoral PK modeling of gefitinib in athymic mice bearing intracerebral U87vIII tumors following either 50 mg/kg or 150 mg/kg single oral doses. The model predicted (—, 50 mg/kg; ---, 150 mg/kg) and observed (Mean + or − SD) (n=3) (●, 50 mg/kg; ▲, 150 mg/kg) gefitinib concentrations are presented for **A.** plasma, **B.** Low MPI tumor group, **C.** Medium MPI tumor group, and **D.** High MPI tumor group.

Table 1

PK and PD model variables of gefitinib determined in mice bearing intracerebral U87vIII tumors. A. Systemic PK parameters, B. Brain tumor PK parameters in regions corresponding to low (less intact BBB), medium and high MPI (more intact BBB) regions and C. PD model variables related to pERK inhibition. Values represent mean (% Coefficient of variation) of model fitted variables unless otherwise stated.

A

Variables	Units	Values
F		0.50 *
V_c	**ml**	69.41 (15%)
k_{10}	**1/hr**	0.31 (17%)
K_a	**1/hr**	0.88 *
$k_{2,1}$	**1/hr**	0.26 (38%)
$k_{1,2}$	**1/hr**	0.30 (59%)

B

Variables	Units	High MPI group	Medium MPI group	low MPI group
K_p	**ml/hr**	0.0024 (23%)	0.0022 (18%)	0.0012 (68%)
Km	**ng/g**	2026.65 (10%)	2048.51 (10%)	2003.35 (10%)
Vmax	**ng/hr**	20.07 (29%)	18.27 (23%)	6.47 (55%)
h	**ml/hr**	0.0006 (63%)	0.0009 (37%)	0.005 (34%)
R*	**-**	2	2	2
Qt*	**ml/hr**	3	3	3
Vt*	**ml**	0.001	0.001	0.001
AUC high dose$_{(0–24)}$	**hr*ng/g**	1.68E+05	1.67E+05	1.70E+05
AUC low dose$_{(0–24)}$	**hr*ng/g**	2.27E+04	2.54E+04	4.91E+04

C

Variables	Units	Value	
		High Dose Model	**Low Dose Model**
IC50	**ng/g**	41969.54 (44%)	16073.65 (42%)
k *	**1/hr**	1	1
K_{in}	**1/hr**	2.02 (11%)	2.02 *
k_{out}	**1/hr**	2.58 (10%)	2.74 (5%)
k_{tr}	**1/hr**	0.32 (18%)	1.34 (16%)
Predicted ABEC (High MPI group)	*a*	9.53	7.57
Predicted ABEC (Medium MPI group)	*a*	9.48	7.64
Predicted ABEC (Low MPI group)	*a*	9.72	8.45

* Values fixed either based on literature or experimentally determined values.

a units of ABEC: (Fraction of baseline pERK * time (hr))

* The parameter “k” was used to link gefitinib tumor concentrations to the pEGFR target compartment and fixed at a value of 1.